Planet. Space Sci., Vol. 35, No. 11, pp. 1389–1395, 1987
Printed in Great Britain.

0032-0633/87 $3.00+0.00

MESOSPHERIC 5577Å GREEN LINE AND ATMOSPHERIC MOTIONS—*ATMOSPHERE EXPLORER* SATELLITE OBSERVATIONS

J. H. YEE and V. J. ABREU
Space Physics Research Laboratory, University of Michigan, Ann Arbor, MI 48109, U.S.A.

(*Received* 10 *April* 1987)

Abstract—Photometric measurements of the 5577Å O(^{1}S) green line mesospheric emission obtained by the Visible Airglow Experiment (VAE) on board the *Atmosphere Explorer* (*AE*) satellite have been analyzed. The inverted volume emission rate profiles showed a peak at approximately 96–97 km with a half-width of ~8 km. The diurnal variation of the intensity indicates the presence of a wave component with 10 ~ 12 h period, probably of solar semi-diurnal tide. Shorter time scale variations due to the presence of travelling waves were also observed.

1. INTRODUCTION

Atmospheric motions induce relative variations of density and temperature between 80 and 100 km altitudes. The airglow emissions originating in this region, such as the O(^{1}S) green line, OH-Meinel band, and O_2 Atmospheric band, thus show some degree of variation in their intensities (Frederick, 1979). The signature of the dynamical processes in this region can then be observed through the emission intensity variation.

Of all the features of airglow emissions in the lower thermosphere and upper mesosphere the diurnal variation of the O(^{1}S) green line has been studied most extensively. Rayleigh (1929) reported the occurrence of a maximum in the 5577Å intensity in the mid-latitude winter night. The diurnal variation later was found to have different behaviours with season, showing an intensity maximum before and after midnight in autumn and spring, respectively (Silverman, 1969). Because such intensity variations cannot be accounted for by photochemical processes, dynamic phenomena such as tides have been invoked (Petitdidier and Teitelbaum, 1976, 1979; Fukuyama, 1976). Shorter scale intensity variations have also been observed and are generally considered to be gravity waves (Korobeynikova and Nasirov, 1976; Teitelbaum and Petitdidier, 1978; Armstrong, 1982; Takahashi *et al.*, 1985). Very short period fluctuations are due to eddy mixing in a region where the gradient of atomic oxygen concentration is rather unimportant (Barat *et al.*, 1972). Recently, Garcia and Solomon (1985) were able to explain the zonally-averaged seasonal and latitudinal variations of the 5577Å emission intensities as observed by the *ISIS* satellite (Cogger *et al.*, 1981), by considering the influence of breaking gravity waves. In brief, dynamical processes in the upper mesosphere and lower thermosphere induce fluctuations in vertical transport, density and temperature, which affect the intensity of the green line nightglow.

In this study, we have analyzed the photometric measurements obtained by the Visible Airglow Experiment (Hays *et al.*, 1973) on board the *Atmosphere Explorer* (*AE*)-*E* satellite. By correcting for the field-of-view and spinning broadening effects, we were able to deduce the mesospheric 5577Å volume emission rate profile from a set of zenith-scanned line-of-sight brightness measurements taken near the perigee altitude of 140 km. Volume emission rate profiles with good vertical resolution, however, can only be obtained when the satellite is near perigee altitudes. Since most of the VAE data were taken while the satellite was above 250 km, in order to include these data in our analysis, we have developed a technique in which measurements made at different satellite altitudes and zenith angles are mapped into corresponding zenith intensities. This technique is based on the assumption that the shape of the volume emission rate profile does not change in space and time and is the one obtained from the inversion of the perigee measurements. The result of our analysis is a morphological map of the mesospheric 5577Å emission.

We also explored the capability of monitoring wave activity in the green line emission intensity from satellite photometric observations and determined

the signature of dynamical processes on the deduced zenith intensities. An example of wave propagation in the mesosphere is presented.

2. DATA ANALYSIS

The Visible Airglow Experiment (VAE) measures surface brightness, i.e. the integrated volume emission rate along the line of sight of the observation. The 5577Å green line during the night at mid-latitude has a maximum emission rate at an altitude near 97 km with a vertical half width equal to about 10 km. The *AE* satellite was spin-stabilized with its spinning axis perpendicular to the orbital plane so that the VAE photometer is able to scan the emission layer at different photometer zenith angles (PZA) or tangent heights. Figure 1 demonstrates the VAE viewing geometry. The VAE photometer has two distinct optical channels, a high-sensitivity channel with a large field of view and a low-sensitivity one with a narrow field of view. The narrow angle channel was designed for limb-scanning experiments and was therefore used in this study. First, we will discuss the technique used to determine the volume emission rate profile from satellite perigee observations.

2.1. *Volume emission rate profile*

Figure 2 shows the observed line-of-sight intensity as a function of photometer zenith angle (PZA) for *AE-E* orbit 1174 while the satellite was near its perigee around 140 km. The local time was near 22:00 h. The photometer zenith angles are corrected by requiring that peak intensities measured in the forward and backward directions occur at the same angle from the vertical. This method allows us to correct for small errors in attitude data, which varies between 1.5° and 1.65° in all the orbits used in this study. A well-defined layer of mesospheric 5577Å emission was observed near the photometer zenith angle of ~97°. At night the emission of thermospheric origin (i.e. produced from dissociative recombination of O_2^+ ions) is situated well above 200 km. Hence near perigee the photometer may view the O(^{1}S) mesospheric emission with minimal interference from the high altitude emission. Its contribution along with the galactic background can then be determined by averaging the measured brightness between PZA of 90° and 95°. For this orbit, it constitutes a brightness of about 200 Rayleighs (R).

In the ideal case, the measured line-of-sight intensity profile, after subtracting for the background emis-

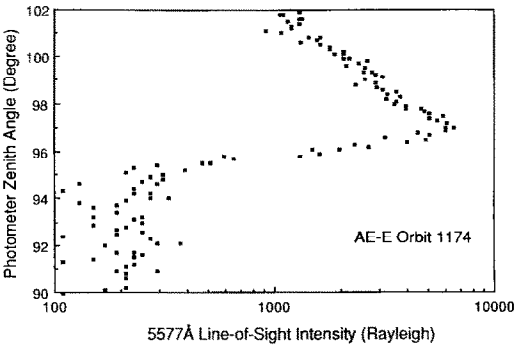

FIG. 2. LINE-OF-SIGHT BRIGHTNESS AS A FUNCTION OF PHOTOMETER ZENITH ANGLE (PZA) FOR *AE-E* ORBIT 1174.

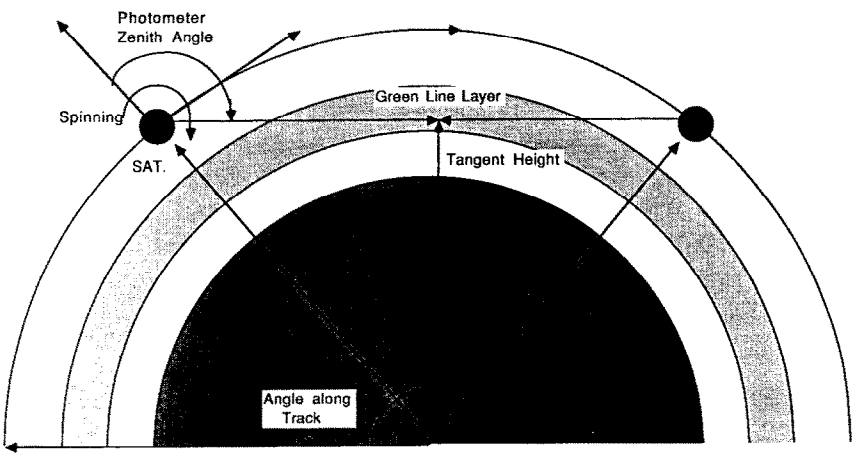

FIG. 1. VIEWING GEOMETRY OF VAE PHOTOMETER IN A SPINNING MODE.

sion, could be used to deduce the volume emission rate profile. The instrument field of view (broadening) and spinning of the satellite (smearing), however, prevent measurements with high vertical resolution. The measured surface brightness $4\pi I_m(\theta)$ for photometer zenith angle θ is then related to the true brightness $4\pi I(\theta)$ by

$$4\pi I_m(\theta) = \int_{\theta - 1/2\omega\tau}^{\theta + 1/2\omega\tau} S(\theta')\, d\theta' \int_{\theta' - \Delta\theta'}^{\theta' + \Delta\theta'} \times W(\theta'' - \theta') 4\pi I(\theta'')\, d\theta'' \quad (1)$$

where $S(\theta)$ and $W(\theta)$ are the broadening functions due to smearing and field-of-view effects, respectively. Here, $\Delta\theta$ is the extent of the off-optical-axis angle integration or three times the half angle width of the photometer channel (3/4°), ω is the satellite spinning rate (24° s^{-1}) and τ is the integration period (32 ms). The true brightness $4\pi I$, measured in Rayleighs, is defined as

$$4\pi I(\theta) = 10^{-6} \int_0^{\infty} \eta(s')\, ds' \quad (2)$$

where η is the volume emission rate at a point s' along the line of sight. For a spherically stratified emission layer,

$$4\pi I(\theta) = 2 \times 10^{-6} \int_{r_0 \sin\theta}^{\infty} \frac{r\eta(r)}{(r^2 - r_0^2 \sin^2\theta)^{1/2}}\, dr \quad (3)$$

where $r_0 = r_s + z$ with r_s being the radius of the Earth and z being the satellite altitude.

Measurements of $4\pi I_m$ can then be inverted from equations (1) and (3) to yield the volume emission rate profile, $\eta(r)$. There are several methods which may be useful in solving this inversion problem, such as the Abel inversion formula used in VAE data production (Hays *et al.*, 1973). They however do not take into account the effects of field-of-view broadening and smearing from satellite spin (equation 1). Here, we use a constrained linear deconvolution (CLD) matrix inversion technique to retrieve $\eta(r)$.

If we denote the set of surface brightness measurements as a column matrix **b** and express the integrations in matrix forms, equations (1) and (3) can be combined as

$$\mathbf{b} = \mathbf{S} * \mathbf{W} * \mathbf{G} * \boldsymbol{\eta} \quad (4)$$

where **G** is the geometric weighting matrix calculated from equation (3); **S** and **W** are the pre-calculated weighting matrices for smearing and field-of-view broadening, respectively. The volume emission rate profile, η, can then be obtained by using an iterative refinement of the linear least-squares method (Bjorck, 1968), with the constrains that all ηs be positive and have only one maximum.

Figures 3a and 3b present the inverted volume emission rate profile for the orbit 1174 and the comparison between the calculated and the observed line-of-sight intensity profiles. The emission rate profiles inverted from the measurements of orbits 1202 and 1413 are also presented in Fig. 3. It shows that the 5577Å mesospheric emission layer has a maximum at an altitude of 97 ± 1 km with a half-width of about 8 km, which agrees very well with past rocket measurements (cf. Bates, 1978).

Given a volume emission rate altitude profile, the measured line-of-sight intensities are different while observing at different directions and from different satellite altitudes. Analysis of satellite data taken at different satellite altitudes thus should either be performed on the inverted volume emission rates or on the normalized intensities, such as the zenith intensities, based upon *a priori* knowledge of how the line-

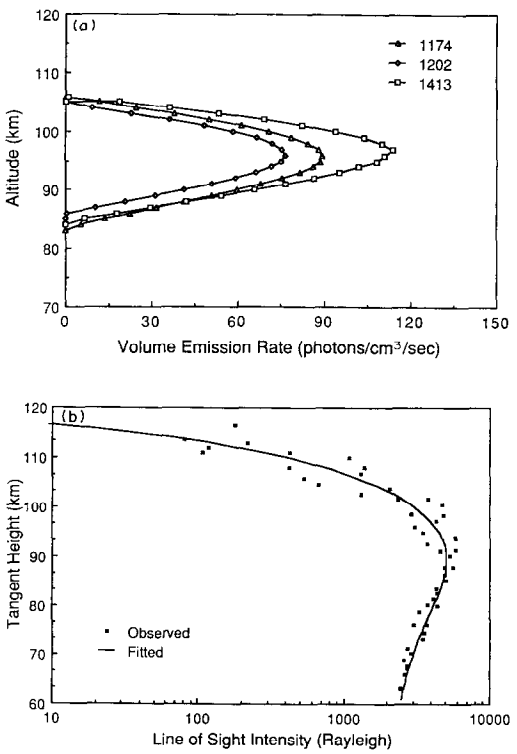

FIG. 3. (a) VOLUME EMISSION RATE PROFILES INVERTED FROM MEASUREMENTS OF *AE-E* ORBIT 1174, 1202 AND 1413, AND (b) THE COMPARISON BETWEEN THE CALCULATED AND THE MEASURED LINE-OF-SIGHT BRIGHTNESS PROFILES FOR ORBIT 1174.

of-sight intensity varies with satellite altitude. Because of the field-of-view broadening and smearing of the VAE photometer, the inversion technique used to obtain a volume emission rate profile works best only while the satellite was below 150 km. The *AE-E* satellite changed to circular orbits at altitudes varying from 250 to 450 km 10 months after its launch and stayed in circular orbits for approximately 4 y. Most of the measurements of 5577Å emission thus were taken above 250 km. Consequently, in order to use the available data to study the morphology of the emission, we have mapped the observations from higher altitudes at different zenith angle into corresponding zenith intensities.

2.2. *Zenith intensity*

Figure 4 shows the simulated line-of-sight intensity profiles of 5577Å nightglow as viewed from three different satellite altitudes, 150, 250 and 350 km. A normalized volume emission rate profile presented in Fig. 3a which gives a zenith brightness of 100 R was used in the simulation. It shows that, as the satellite altitude increases, the peak intensity becomes smaller and appears at a lower tangent height. The simulated intensity profiles can then be used to convert each line-of-sight measurement taken at various spacecraft altitudes and photometer zenith angles to a corresponding zenith intensity at the tangent point.

Figure 5 shows the line-of-sight measurements of orbit 7074 obtained at a satellite altitude of 251 km. The galactic background and the thermospheric emission brightness, instead of being an averaged constant value as in the previous case, was determined by linearly fitting the measurements as a function of photometer zenith angle and has subsequently been subtracted. The zenith intensity was least-square fitted to be 267 R, and the calculated line-of-sight

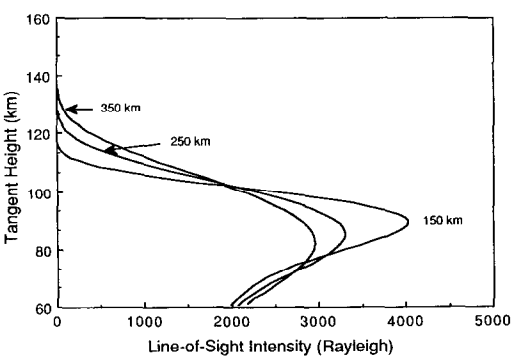

FIG. 4. CALCULATED LINE-OF-SIGHT BRIGHTNESS PROFILES AS VIEWED FROM THREE DIFFERENT SPACECRAFT ALTITUDES.

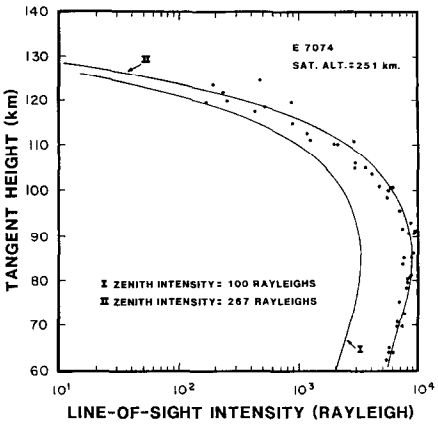

FIG. 5. COMPARISON BETWEEN THE FITTED AND MEASURED LINE-OF-SIGHT BRIGHTNESS PROFILES FOR ORBIT 7074. The satellite altitude was 251 km.

intensity profile, as it is plotted in Fig. 5, agrees very well with the observations.

The technique just described assumes that the horizontal distribution of the emission layer is uniform and that the measured intensity mainly results from the region near the tangent point. In fact, if horizontal structure were present in the emission layer in the form of an oscillation, it would be smeared by the line-of-sight viewing geometry. The degree of smearing depends upon the nature of the emission horizontal structure and the viewing geometry. Simulations were therefore performed to examine how the horizontal structure is recovered from line-of-sight measurements.

2.3. *Data simulation*

The simulations were performed using the technique described above for two different spatial variations in the green line intensity: one having a large-scale oscillation with period of 120° in angle along the satellite track and the other having a medium-scale oscillation with period of 30°. In the simulations the emission is measured at three zenith angles, 102°, 103° and 104° from an orbital altitude of 250 km, or at tangent heights of 105, 80 and 52 km, respectively. The recovered zenith intensities from these three sets of line-of-sight measurements are shown in Figs 6a and 6b. The large-scale wave structure can be recovered successfully from all three zenith angle line-of-sight measurements, but the intensity of the higher frequency wave can only be recovered when the zenith angle of observations is less than ~103° (tangent height ~80 km). A slight shift (~1°) can be observed

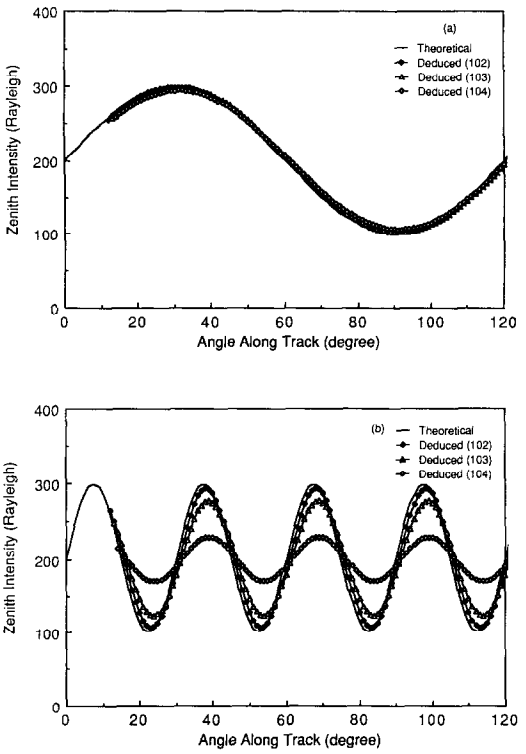

FIG. 6. DEDUCED ZENITH INTENSITIES FROM SIMULATED VAE MEASUREMENTS AT THREE DIFFERENT ZENITH ANGLES (102°, 103° AND 104°) FROM AN ORBIT OF 250 km FOR INTENSITY VARIATIONS OF (a) A LARGE-SCALE WAVE, AND (b) A MEDIUM-SCALE WAVE.

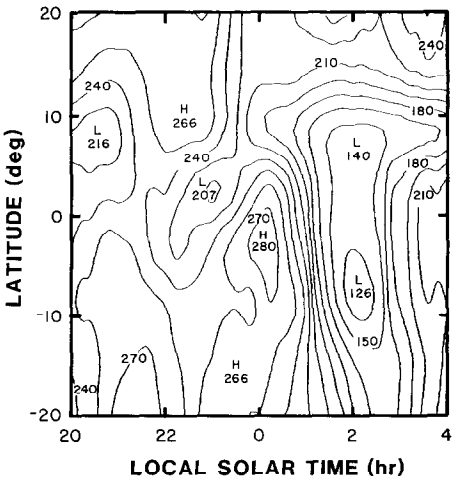

FIG. 7. CONTOUR OF THE 5577Å NIGHTGLOW ZENITH INTENSITY IN THE EQUINOX AS A FUNCTION OF LOCAL SOLAR TIME AND LATITUDE.

in the recovered high frequency wave, but in general, this is not important in our data analysis. In this study, therefore, measurements with tangent heights less than 80 km have been excluded, and any wave features with frequencies higher than the medium-scale wave simulated here would have been smeared.

3. RESULTS

Figure 7 shows a contour of the deduced 5577Å nightglow zenith intensity in the spring equinox condition as a function of local solar time and latitude. Due to the large variation in solar inclination angles during the spring months, only orbits in the months of March and early April (6 in 1977 and 20 in 1980) have been analyzed to study the morphology of 5577Å emission in the equinox condition. Measurements taken during twilight were rejected if the photometer was looking into the daytime atmosphere, in order to avoid possible errors in the thermospheric emission correction due to its large variability. Also because of the inclination of *AE-E* orbits, the measurements were confined within 20° of the geographic equator. The map indicates that the 5577Å emission has a strong post-sunset maximum near 21:00 h with a zenith intensity of ~250 R within 10°–20° latitudes at both sides of the equator. This maximum is followed by a post-midnight minimum near 02:00 h, clearly appearing in the Northern Hemisphere, with an intensity of ~ 150 R. Superimposed on this general feature are wave structures of shorter scale which become very important near the equator.

Figure 8 shows the 5577Å nightglow zenith intensity averaged over latitude as a function of local solar time. A wave component with a period of 10–12 h seems to be responsible for the observed local time dependence. This agrees well with the suggestion by Petitdidier and Teitelbaum (1976, 1979) that the behaviour of the average diurnal variation of 5577Å intensity may be explained by the solar semi-diurnal tide.

Figure 9 presents the 5577Å zenith intensity averaged over solar local time as a function of latitude in the equinox condition. Although the variances are largely due to its large local solar time variation, the averaged green line intensity appears to be weaker near the geographic equator. This agrees with the results obtained by the *ISIS* satellite (Cogger *et al.*, 1981) and the model calculation by Garcia and Solomon (1985) in which the effect of breaking gravity waves in the mesosphere is considered. The green line

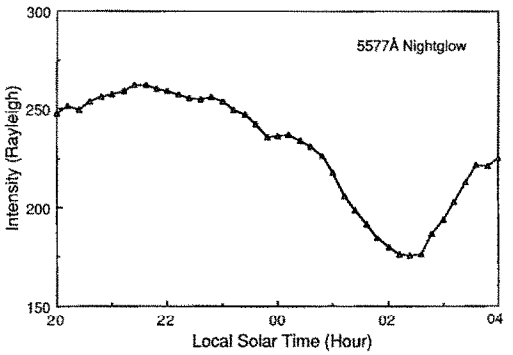

FIG. 8. LATITUDINALLY-AVERAGED ZENITH INTENSITY AS A FUNCTION OF LOCAL SOLAR TIME.

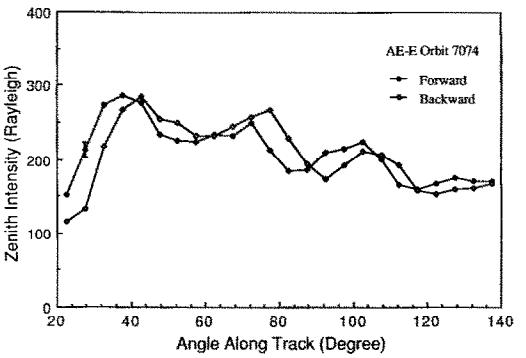

FIG. 10. DEDUCED ZENITH INTENSITY AS A FUNCTION OF TANGENT POINT LOCATION ALONG ORBIT 7074 FOR BOTH FORWARD- AND BACKWARD-LOOKING MEASUREMENTS.

intensities we obtained were slightly larger than the *ISIS* measurements, probably due to a solar activity effect (Takahashi *et al.*, 1984) since most of our data were taken during active solar periods (March of 1980).

When the satellite is in the spinning mode, VAE performs two limb-scanning measurements, one forward and one backward, during each 15-s revolution. This provides us with a unique opportunity to measure the emission from the same volume in space from a set of forward- and backward-looking observations several minutes apart (Fig. 1), and to examine the short-scale temporal variation of emission intensity. The time separation between the two observations is determined by the orbital altitude.

Wave structures of shorter time scale are most frequently seen in each individual orbit. Figure 10 shows the deduced zenith intensities as a function of the tangent point location, represented by the angle along the satellite track, for both forward- and backward-looking measurements along orbit 7074. The satellite in this orbit was at $\sim$250 km altitude, thus the forward-looking measurements led the backward measurements in time by approximately 6 min. A constant shift ($\sim 6^\circ$ in angle-along-track) can be found between the forward- and backward-looking data, indicating the presence of a wave propagation in the emission altitudes. Assuming the wave is traveling horizontally, its wavelength can then be estimated to be 30° in angle along satellite track, or $\sim$3500 km. This only represents an upper limit, and the real wavelength would depend upon the orientation of the satellite track with respect to the wave front. A wave which travels $\sim 6^\circ$ in angle along the satellite track in 6 min (the slowest possible traveling wave in this case) is estimated to have a wave period about 30–40 min and a phase speed of ~ 1 km s^{-1}. The apparent phase speed determined here is substantially faster than the speed of sound, therefore is almost certainly incorrect. Factors that might contribute to an error in phase speed are our lack of knowledge of the true horizontal wavelength and an assignment of the signal to the wrong tangent point, caused by our data analysis technique and a distortion of the volume emission rate profile in the presence of a wave. Identifying the characteristics of the traveling wave considered here therefore is difficult, and a dynamical/chemical model of the airglow emission in this region is required to further interpret our results.

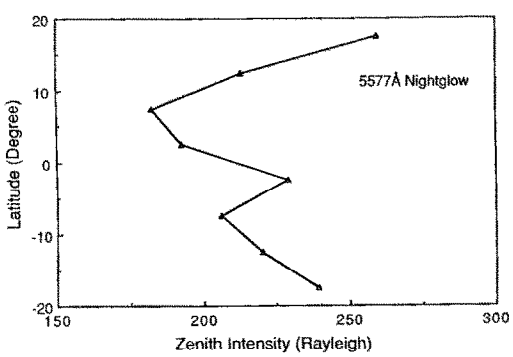

FIG. 9. NIGHT-TIME AVERAGED ZENITH INTENSITY AS A FUNCTION OF LATITUDE.

Acknowledgements—This research was supported at the University of Michigan by NASA grants NAGW-496 and NAS5-27751.

REFERENCES

Armstrong, E. B. (1982) The association of visible airglow features with a gravity wave. *J. atmos. terr. Phys.* **44**, 325.

Barat, J., Blamont, J. E., Petitdidier, M., Sidi, C. and Teitelbaum, H. (1972) Mise en évidence expérimentale d'une structure inhomogène petite échelle dans la couche émissive de l'oxygène atomique à 5577Å. *Annls geophys.* **28,** 145.

Bates, D. R. (1978) Forbidden oxygen and nitrogen lines in the nightglow. *Planet. Space Sci.* **26**, 897.

Bjorck, Å. (1968) Iterative refinement of linear least squares solutions II. *BIT* **8**, 8.

Cogger, L. L., Elphinstone, R. D. and Murphree, J. S. (1981) Temporal and latitudinal 5577Å airglow variations. *Can. J. Phys.* **59**, 1296.

Frederick, J. E. (1979) Influence of gravity wave activity on lower thermospheric photochemistry and composition. *Planet. Space Sci.* **27**, 1469.

Fukuyama, K. (1976) Airglow variations and dynamics in the lower thermosphere and upper mesosphere—I. Diurnal variations and its seasonal dependency. *J. atmos. terr. Phys.* **38**, 1279.

Garcia, R. R. and Solomon, S. (1985) The effect of breaking gravity waves on the dynamics and chemical composition of the mesosphere and lower thermosphere. *J. geophys. Res.* **90**, 3850.

Hays, P. B., Carignan, G., Kennedy, B. C., Shepherd, G. G. and Walker, J. C. G. (1973) The visible airglow experiment on *Atmosphere Explorer*. *Radio Sci.* **8**, 369.

Korobeynikova, M. P. and Nasirov, G. A. (1976) Influence of the internal gravity waves on the behaviour of the nightglow emission 557.7 nm. *Annls geophys.* **32**, 39.

Petitdidier, M. and Teitelbaum, H. (1976) Lower thermosphere emissions and tides. *Planet. Space Sci.* **27**, 1409.

Petitdidier, M. and Teitelbaum, H. (1979) $O(^1S)$ excitation mechanism and atmospheric tides. *Planet. Space Sci.* **27**, 1409.

Rayleigh, R. J. (1929) A photoelectric method of measuring the light of the night sky with studies of the course of variation through the night. *Proc. R. Soc.* **A124**, 395.

Silverman, S. M. (1969) *Atmospheric Emissions* (Edited by McCormac, B. M), p. 383 . Van Norstrand, New York.

Takahashi, H., Batista, P. P., Sahai, Y. and Clemesha, B. R. (1985) Atmospheric wave propagations in the mesopause region observed by the OH(8,3) band, NaD, O_2A (8645 Å) band and OI 5577 Å nightglow emissions. *Planet. Space Sci.* **33**, 1985.

Takahashi, H., Sahai, Y. and Batista, P. P. (1984) Tidal and solar cycle effects on the OI 5577 Å, NaD and OH(8,3) airglow emissions observed at 23°S. *Planet. Space Sci.* **32**, 897.

Teitelbaum, H. and Petitdidier, M. (1978) Night-time variation of short period fluctuations (2–15 min) in the oxygen green line. *J. atmos. terr. Phys.* **430**, 223.